Surface lattice resonances strongly coupled to Rhodamine 6G excitons: tuning the plasmon-exciton-polariton mass and composition

S.R.K. Rodriguez [1,*] **and J. Gómez Rivas** [2]

[1] *Center for Nanophotonics, FOM Institute AMOLF, c/o Philips Research Laboratories, High Tech Campus 4, 5656 AE Eindhoven, The Netherlands*

[2] *COBRA Research Institute, Eindhoven University of Technology, P.O. Box 513, 5600 MB Eindhoven, The Netherlands*

s.rodriguez@amolf.nl

Abstract: We demonstrate the strong coupling of surface lattice resonances (SLRs) — hybridized plasmonic/photonic modes in metallic nanoparticle arrays — to excitons in Rhodamine 6G molecules. We investigate experimentally angle-dependent extinction spectra of silver nanorod arrays with different lattice constants, with and without the Rhodamine 6G molecules. The properties of the coupled modes are elucidated with simple Hamiltonian models. At low momenta, plasmon-exciton-polaritons — the mixed SLR/exciton states — behave as free-quasiparticles with an effective mass, lifetime, and composition tunable via the periodicity of the array. The results are relevant for the design of plasmonic systems aimed at reaching the quantum degeneracy threshold, wherein a single quantum state becomes macroscopically populated.

OCIS codes: (240.6680) Surface plasmons; (230.4555) Coupled resonators; (050.1970) Diffractive optics; (240.5420) Polaritons.

References and links

1. P. Mühlschlegel, H.-J. Eisler, O. J. F. Martin, B. Hecht, and D. W. Pohl, "Resonant optical antennas," Science **308**, 1607–1609 (2005).
2. P. Bharadwaj, B. Deutsch, and L. Novotny, "Optical antennas," Adv. Opt. Photon. **1**, 438–483 (2009).
3. A. G. Curto, G. Volpe, T. H. Taminiau, M. P. Kreuzer, R. Quidant, and N. F. van Hulst, "Unidirectional emission of a quantum dot coupled to a nanoantenna," Science **329**, 930–933 (2010).
4. P. Berini, "Plasmon polariton modes guided by a metal film of finite width," Opt. Lett. **24**, 1011–1013 (1999).
5. W. L. Barnes, A. Dereux, and T. W. Ebbesen, "Surface plasmon subwavelength optics," Nature (London) **424**, 824–830 (2003).
6. E. Moreno, S. G. Rodrigo, S. I. Bozhevolnyi, L. Martín-Moreno, and F. J. García-Vidal, "Guiding and focusing of electromagnetic fields with wedge plasmon polaritons," Phys. Rev. Lett. **100**, 023901 (2008).
7. K. T. Carron, W. Fluhr, M. Meier, A. Wokaun, and H. W. Lehmann, "Resonances of two-dimensional particle gratings in surface-enhanced raman scattering," J. Opt. Soc. Am. B **3**, 430–440 (1986).
8. S. Zou and G. C. Schatz, "Narrow plasmonic/photonic extinction and scattering line shapes for one and two dimensional silver nanoparticle arrays," J. Chem. Phys. **121**, 12606–12612 (2004).
9. E. M. Hicks, S. Zou, G. C. Schatz, K. G. Spears, R. P. Van Duyne, L. Gunnarsson, T. Rindzevicius, B. Kasemo, and M. Käll, "Controlling plasmon line shapes through diffractive coupling in linear arrays of cylindrical nanoparticles fabricated by electron beam lithography," Nano Lett. **5**, 1065–1070 (2005).
10. F. J. García de Abajo, "Colloquium: Light scattering by particle and hole arrays," Rev. Mod. Phys. **79**, 1267–1290 (2007).

#195021 - $15.00 USD Received 31 Jul 2013; revised 23 Sep 2013; accepted 24 Sep 2013; published 4 Nov 2013

11. Y. Chu, E. Schonbrun, T. Yang, and K. B. Crozier, "Experimental observation of narrow surface plasmon resonances in gold nanoparticle arrays," Appl. Phys. Lett. **93**, 181108 (2008).
12. B. Auguié and W. L. Barnes, "Collective resonances in gold nanoparticle arrays," Phys. Rev. Lett. **101**, 143902 (2008).
13. V. G. Kravets, F. Schedin, and A. N. Grigorenko, "Extremely narrow plasmon resonances based on diffraction coupling of localized plasmons in arrays of metallic nanoparticles," Phys. Rev. Lett. **101**, 087403 (2008).
14. G. Vecchi, V. Giannini, and J. Gómez Rivas, "Surface modes in plasmonic crystals induced by diffractive coupling of nanoantennas," Phys. Rev. B **80**, 201401 (2009).
15. S. R. K. Rodriguez, A. Abass, B. Maes, O. T. A. Janssen, G. Vecchi, and J. Gómez Rivas, "Coupling bright and dark plasmonic lattice resonances," Phys. Rev. X **1**, 021019 (2011).
16. W. Zhou and T. W. Odom, "Tunable subradiant lattice plasmons by out-of-plane dipolar interactions," Nature Materials **6**, 423–427 (2011).
17. T. V. Teperik and A. Degiron, "Design strategies to tailor the narrow plasmon-photonic resonances in arrays of metallic nanoparticles," Phys. Rev. B **86**, 245425 (2012).
18. G. Weick, C. Woollacott, W. L. Barnes, O. Hess, and E. Mariani, "Dirac-like plasmons in honeycomb lattices of metallic nanoparticles," Phys. Rev. Lett. **110**, 106801 (2013).
19. S. Rodriguez, M. Schaafsma, A. Berrier, and J. Gómez Rivas, "Collective resonances in plasmonic crystals: Size matters," Physica B: Condensed Matter **407**, 4081 (2012).
20. G. Vecchi, V. Giannini, and J. Gómez Rivas, "Shaping the fluorescent emission by lattice resonances in plasmonic crystals of nanoantennas," Phys. Rev. Lett. **102**, 146807 (2009).
21. V. Giannini, G. Vecchi, and J. Gómez Rivas, "Lighting up multipolar surface plasmon polaritons by collective resonances in arrays of nanoantennas," Phys. Rev. Lett. **105**, 266801 (2010).
22. G. Pellegrini, G. Mattei, and P. Mazzoldi, "Nanoantenna arrays for large-area emission enhancement," J. Phys. Chem. C **115**, 24662–24665 (2011).
23. S. R. K. Rodriguez, G. Lozano, M. A. Verschuuren, R. Gomes, K. Lambert, B. D. Geyter, A. Hassinen, D. V. Thourhout, Z. Hens, and J. G. Rivas, "Quantum rod emission coupled to plasmonic lattice resonances: A collective directional source of polarized light," Appl. Phys. Lett. **100**, 111103 (2012).
24. G. Lozano, D. J. Louwers, S. R.K. Rodriguez, S. Murai, O. T. Jansen, M. A. Verschuuren, and J. Gomez Rivas, "Plasmonics for solid-state lighting: enhanced excitation and directional emission of highly efficient light sources," Light Sci. Appl. **2**, e66 (2013).
25. W. Zhou, M. Dridi, J. Y. Suh, C. H. Kim, D. T. Co, M. R. Wasielewski, G. C. Schatz, and T. W. Odom, "Lasing action in strongly coupled plasmonic nanocavity arrays," Nature Nanotechnology **8**, 506–511 (2013).
26. J. Bellessa, C. Bonnand, J. C. Plenet, and J. Mugnier, "Strong coupling between surface plasmons and excitons in an organic semiconductor," Phys. Rev. Lett. **93**, 036404 (2004).
27. J. Dintinger, S. Klein, F. Bustos, W. L. Barnes, and T. W. Ebbesen, "Strong coupling between surface plasmon-polaritons and organic molecules in subwavelength hole arrays," Phys. Rev. B **71**, 035424 (2005).
28. Y. Sugawara, T. A. Kelf, J. J. Baumberg, M. E. Abdelsalam, and P. N. Bartlett, "Strong coupling between localized plasmons and organic excitons in metal nanovoids," Phys. Rev. Lett. **97**, 266808 (2006).
29. P. Vasa, R. Pomraenke, S. Schwieger, Y. I. Mazur, V. Kunets, P. Srinivasan, E. Johnson, J. E. Kihm, D. S. Kim, E. Runge, G. Salamo, and C. Lienau, "Coherent exciton-surface-plasmon-polariton interaction in hybrid metal-semiconductor nanostructures," Phys. Rev. Lett. **101**, 116801 (2008).
30. T. K. Hakala, J. J. Toppari, A. Kuzyk, M. Pettersson, H. Tikkanen, H. Kunttu, and P. Törmä, "Vacuum rabi splitting and strong-coupling dynamics for surface-plasmon polaritons and rhodamine 6g molecules," Phys. Rev. Lett. **103**, 053602 (2009).
31. N. I. Cade, T. Ritman-Meer, and D. Richards, "Strong coupling of localized plasmons and molecular excitons in nanostructured silver films," Phys. Rev. B **79**, 241404 (2009).
32. A. Manjavacas, F. Garcia de Abajo, and P. Nordlander, "Quantum plexcitonics: Strongly interacting plasmons and excitons," Nano Lett. **11**, 2318–2323 (2011).
33. T. Schwartz, J. A. Hutchison, C. Genet, and T. W. Ebbesen, "Reversible switching of ultrastrong light-molecule coupling," Phys. Rev. Lett. **106**, 196405 (2011).
34. A. González-Tudela, P. A. Huidobro, L. Martín-Moreno, C. Tejedor, and F. J. García-Vidal, "Theory of Strong Coupling between Quantum Emitters and Propagating Surface Plasmons," Phys. Rev. Lett. **110**, 126801 (2013).
35. M. A. Verschuuren, "Substrate conformal imprint lithography for nanophotonics," PhD dissertation, Utrecht University (2010).
36. A. Wokaun, H.-P. Lutz, A. P. King, U. P. Wild, and R. R. Ernst, "Energy transfer in surface enhanced luminescence," J. Chem. Phys. **79**, 509 (1983).
37. P. Anger, P. Bharadwaj, and L. Novotny, "Enhancement and quenching of single-molecule fluorescence," Phys. Rev. Lett. **96**, 113002 (2006).
38. B. Wiley, Y. Sun, and Y. Xia, "Synthesis of silver nanostructures with controlled shapes and properties," Acc. Chem. Res. **40**, 1067–1076 (2007).
39. H. Deng, H. Haug, and Y. Yamamoto, "Exciton-polariton Bose-Einstein condensation," Rev. Mod. Phys. **82**, 1489–1537 (2010).

#195021 - $15.00 USD Received 31 Jul 2013; revised 23 Sep 2013; accepted 24 Sep 2013; published 4 Nov 2013

40. J. J. Hopfield, "Theory of the contribution of excitons to the complex dielectric constant of crystals," Phys. Rev. **112**, 1555–1567 (1958).

1. Introduction

Metallic nanostructures hold fascinating optical properties associated with the excitation of surface electromagnetic modes at the air-dielectric interface. These modes are known as surface plasmon polaritons (SPPs), and they exist in essentially two types: localized and propagating. Localized SPPs typically lead to a strong confinement of radiation in sub-wavelength volumes, making them ideal candidates for nanoscale optical antennas [1–3]. On the other hand, propagating SPPs typically display subwavelength confinement in 1 or 2 spatial dimensions only, while they transport energy in the other dimension(s) [4–6]. Periodic arrays of metallic nanoparticles constitute an interesting system in which these two types of modes co-exist. Localized surface plasmon resonances (LSPRs) in the nanoparticles may couple to diffracted orders in the plane of the array, so-called Rayleigh anomalies, leading to mixed plasmonic/photonic states with variable degree of localization. These hybrid states are known as surface lattice resonances (SLRs).

SLRs were pioneered in the context of surface-enhanced Raman spectroscopy by Carron and co-workers [7]. They were later re-fueled by Schatz and co-workers, who predicted extremely sharp resonance linewidths ($\sim$ 1 meV) near the diffraction edge of metallic nanoparticle arrays [8]. Since then, a large number of theoretical and experimental studies have been performed on these hybrid modes [9–18]. Interest in SLRs has been largely driven by their collective character, which enables the excitation of highly delocalized surface modes in the plane of the array with subwavelength confinement out of the plane of the array [14,19]. Furthermore, these features can be tuned by structural design of the nanoparticles and of the lattice, as these determine the SLR linewidth and dispersion [15,17]. With such a versatile system, the possibilities to tailor the emission from extended sources (e.g. thin layers of luminescent molecules or quantum dots) are many [20–24]. Previous work in this direction has focused on the interaction of SLRs with luminescent excitons in the weak coupling regime, which can even lead to photon lasing [25]. While several landmark papers have discussed the plasmon-exciton strong coupling in various plasmonic systems [26–34], the SLR-exciton strong coupling remains unexplored.

In this paper we investigate the strong coupling of SLRs in arrays of silver nanorods to excitons in Rhodamine 6G (R6G) molecules. We present experimental results for three arrays having identical nanorods but varying lattice constants. Different SLR-exciton detunings are probed in each array by energy-momentum spectroscopy, as the steep dispersion band of the bare SLR crosses the flat dispersion band of the bare exciton. We focus on the low-energy band of the strongly coupled modes which anti-cross: "plasmon-exciton-polaritons" (PEPs). At low momenta PEPs effectively behave as free-quasiparticles, with mass, lifetime, and composition (the relative weights of SLR and exciton constituents in the admixture) tunable via the periodicity of the array. These results have implications for reaching the (yet unreported) quantum degeneracy threshold in plasmonic systems. For instance, as quantum condensation occurs when the de Broglie wavelength ($\Lambda \propto 1/\sqrt{mk_BT}$ with m the mass, k_B Boltzmann's constant, and T the temperature) exceeds the interparticle separation, a reduction in polariton mass is expected to increase the critical temperature for condensation at a given density of quasiparticles.

2. Sample preparation and experimental methods

Silver nanorod arrays were fabricated onto a fused silica substrate by substrate conformal imprint lithography: a technique enabling accurate reproduction of nanoscale features over large ($>$cm^2) areas [35]. A 20 nm layer of Si_3N_4 was deposited on top of the arrays to prevent

#195021 - $15.00 USD Received 31 Jul 2013; revised 23 Sep 2013; accepted 24 Sep 2013; published 4 Nov 2013

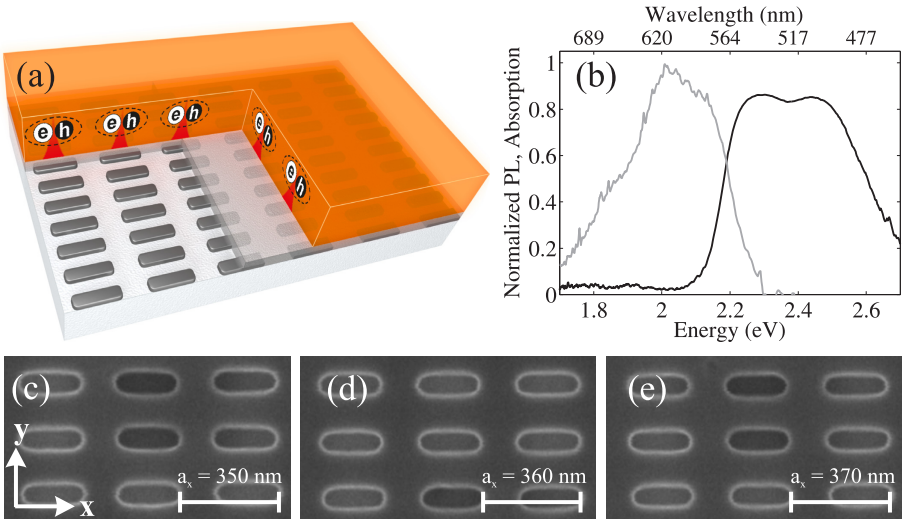

Fig. 1. (a) Schematic representation of a silver nanorod array on an SiO_2 substrate covered by a thin passivating Si_3N_4 layer (gray) and a Rhodamine 6G in PVA layer (orange). (b) Normalized photoluminescence (gray line) and absorptance of a 300 nm layer of Rhodamine 6G in PVA (black line) without the nanorod array. (c)-(e) Scanning electron microscope images of the resist layers used for the fabrication of the nanorod arrays. The scale bars denote the lattice constant which is tuned; other dimensions are fixed.

the silver from oxidizing. The Si_3N_4 also serves as a spacer layer between the nanorods and the organic molecules to avoid emission quenching [36, 37]. Figure 1 shows a 3D inclined representation of the sample. The thin semi-transparent gray layer represents the Si_3N_4. The upper orange layer represents the polyvinyl alcohol (PVA) layer that can have R6G molecules embedded. The R6G excitons are represented by electron-hole pairs enclosed by a dashed ellipse. Figure 1(b) shows the normalized emission (gray line) and absorptance (black line) of a 300 ± 30 nm layer of R6G molecules. Figures 1(c)- 1(e) show scanning electron microscope images of the resist layers used in the fabrication of the arrays. Subsequent processing involved perpendicular evaporation of 20 nm silver and lift-off. All three arrays have nanorods with dimensions $230 \times 70 \times 20$ nm^3, and a lattice constant $a_y = 200$ nm. The lattice constant along the long axis of the nanorods, a_x, is 350 nm in Fig. 1(c), 360 nm in Fig. 1(d), and 370 nm in Fig. 1(e). The tolerances of the in plane dimensions are ± 10 nm, while out of the plane it is ± 2 nm.

We measured the variable angle extinction spectra for all three arrays with and without the R6G molecules. The extinction is given by $1 - T_0$, with T_0 the zeroth order transmittance of a white light beam from a halogen lamp. The incident beam was collimated (angular spread $< 0.1^\circ$) and linearly polarized parallel to the short axis of the nanorods (y-axis). The sample was rotated about the y-axis by a computer controlled rotation stage with an angular resolution of 0.1°. Rotation by an angle θ changed the projection of the incident wave vector parallel to the long axis of the nanorods (x-axis). Namely, $\mathbf{k}_{\|} = \frac{\omega}{c}\sin(\theta)\hat{x}$, with ω the incident frequency, c the vacuum speed of light, and $\hat{x}$ a unit vector along the x-axis.

#195021 - $15.00 USD Received 31 Jul 2013; revised 23 Sep 2013; accepted 24 Sep 2013; published 4 Nov 2013

3. Extinction of nanoparticle arrays without R6G molecules

In Figure 2 we present extinction measurements of the three nanorod arrays previously discussed. All arrays are covered by a 300 nm layer of PVA without R6G molecules. The dispersive peaks in extinction underneath the black lines are SLRs. These are mixed states formed by the strong coupling of localized surface plasmons to Rayleigh anomalies. We illustrate this coupling mechanism with the following simplified 3×3 Hamiltonian,

$$H_1 = \begin{pmatrix} E_L - i\gamma_L & \Omega_{L+} & \Omega_{L-} \\ \Omega_{L+} & E_{R+} - i\gamma_{R+} & \Omega_{\pm} \\ \Omega_{L-} & \Omega_{\pm} & E_{R-} - i\gamma_{R-} \end{pmatrix}. \quad (1)$$

The diagonal terms in the Hamiltonian are the energies of the LSPR and Rayleigh anomalies associated with the $(\pm 1, 0)$ diffraction orders. Their real parts are shown as white lines in Figures 2(a)- 2(c), with the LSPR as a solid line, and the $(\pm 1, 0)$ Rayleigh anomalies as dashed lines. The Rayleigh anomalies are calculated from the conservation of the parallel component of the wave-vector: $E_{R\pm}(k_{\|}) = \frac{\hbar c}{n} \left| k_{\|} + mG_x \right|$. Here, $m = \pm 1$ is the order of diffraction, $G_x = \frac{2\pi}{a_x}$ is the x-component of the reciprocal lattice vector, and $n = 1.47$ is the effective refractive index of the medium in which the mode propagates. The value of n (intermediate between the refractive indices of SiO_2 and PVA) is estimated from the measurements, which display a minimum in extinction at the Rayleigh anomaly condition [15]. As the lattice constant is $a_x = 350$ nm in Fig. 2(a), $a_x = 360$ nm in Fig. 2(b), and $a_x = 370$ nm in Fig. 2(c), the Rayleigh anomalies shift towards lower energies. The real part of the LSPR energy is set to $E_L = 2.5$ eV based on the SLR dispersion, which asymptotically approaches the LSPR energy at large $k_{\|}$ (not shown here). This energy corresponds to the dipolar LSPR along the short axis of the nanorods, and it is in good agreement with the corresponding peak in the scattering spectra of single nanorods with dimensions similar to those herein considered [38]. We set equal LSPR energy for all arrays because the nanorod dimensions are the same.

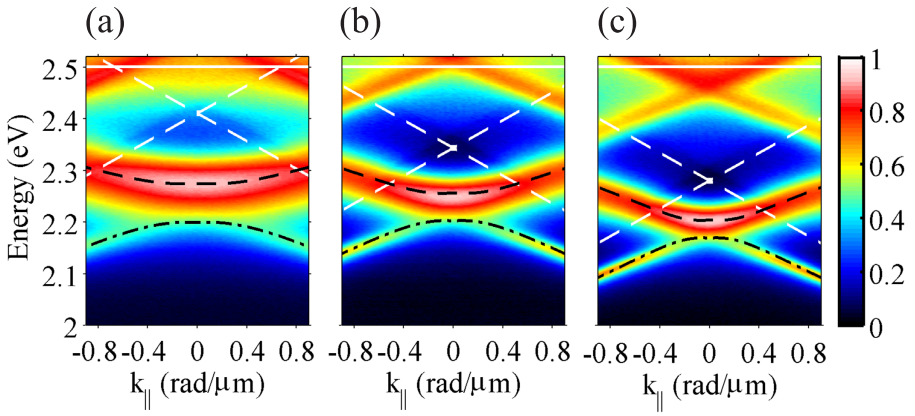

Fig. 2. Extinction —in the same color scale for all plots— as a function of the incident photon energy and wave-vector component parallel to the long axis of the nanorods. The lattice constants are (a) $a_x = 350$ nm, (b) $a_x = 360$ nm, and (c) $a_x = 370$ nm. The nanorod arrays are all covered by a 300 nm PVA layer without R6G molecules. The white lines indicate the energies of the bare states: LSPR as white solid line, and $(\pm 1, 0)$ Rayleigh anomalies as white dashed lines. The black lines indicate the energies of the coupled states: upper SLR as black dashed line and lower SLR as black dash-dotted line.

The imaginary parts of the LSPR and Rayleigh anomaly energies (the time-decay of the

#195021 - $15.00 USD Received 31 Jul 2013; revised 23 Sep 2013; accepted 24 Sep 2013; published 4 Nov 2013

modes) are estimated from the linewidths in the measurements. We take these to be the half-width at half maximum at $k_{\|} = 0$, where the energy detuning of the uncoupled states is largest and the coupled states resemble most the uncoupled ones. The off-diagonal terms in the Hamiltoninan are the coupling constants, which are fitted to match the dispersion measured for each array. Both decay and coupling constants are here assumed to be frequency-independent for simplicity. The values used in the calculations of Fig. 2 are reported in Table 1.

Table 1. Input parameters to the model Hamiltonian in Eq. (1) yielding the eigenenergies in Fig. 2. All quantities are in units of meV.

a_x	Ω_{L+}	Ω_{L-}	$\Omega_{\pm}$	γ_L	γ_{R+} and γ_{R-}
350 nm	210 ± 20	190 ± 20	210 ± 10	140 ± 20	60 ± 10
360 nm	180 ± 20	160 ± 20	140 ± 10	140 ± 20	50 ± 10
370 nm	180 ± 20	160 ± 20	110 ± 10	140 ± 20	40 ± 10

Diagonalization of the the Hamiltonian H_1 in Eq. (1) leads to three new eigenstates. Only two of these states appear in the energy range of the measurements. These are the upper and lower SLRs, which are shown in Fig. 2 as black dashed and dash-dotted lines, respectively. The calculated eigenenergies are in good agreement with the measurements, indicating that the simplified model here employed describes reasonably well the experiments. In our analysis, we have ignored the resonances on the high-energy side of the measurements in Fig. 2 because they represent only a small perturbation to the upper SLR at large $k_{\|}$. Since we are interested in the small $k_{\|}$ regime for the upper SLR (near the ground state), these effects are mostly irrelevant for the purpose of this work.

SLRs display a number of interesting features near $k_{\|} = 0$, which are associated with the coupling of modes with different symmetries [15]. The anti-crossing of the upper and lower SLRs, with an energy gap depending on the geometry of nanorods, is the signature of the SLR mutual coupling described by $\Omega_{\pm}$ [15]. This effect is present in both driven (extinction) and un-driven (eigenenergies) systems. Moreover, the driven system displays an upper SLR with an enhanced extinction at $k_{\|} = 0$ (i.e. a bright state), while the extinction of the lower SLR vanishes (i.e. a dark state). The symmetries of the modes are responsible for bright/dark character of SLRs [15]. The electric field of the upper SLR has even parity about the plane defined by the incident wave and polarization vectors. In contrast, the electric field of the lower SLR has odd parity. This makes the bright ground state of the upper SLR radiatively broadened, while the lower SLR can not be excited by the incident plane wave at $k_{\|} = 0$. The symmetries of these modes are broken for small $k_{\|} \neq 0$, and their radiative losses vary with $k_{\|}$. The $k_{\|}$-dependent radiative losses for the upper SLR will become particularly evident in the next section, where we analyze the linewidths of SLRs strongly coupled to excitons. In what follows, we will concentrate on the upper SLR.

The changes in the SLR group velocity ($\partial E/\partial k_{\|}$) and linewidth are associated with the energy detuning between the LSPR and Rayleigh anomalies. Besides $k_{\|}$, another important detuning parameter is the periodicity of the array, as it determines the relative weights of the LSPR and Rayleigh anomalies in the mixed SLR state at a particular wave vector. Considering the case at $k_{\|} = 0$, we observe in Figs. 2(a)- 2(c) that the SLR linewidth decreases for increased lattice constants. This implies an increase in the lifetime of the excitation and a weaker confinement of the electromagnetic field. Thus, the SLR becomes more "photonic" and less "plasmonic" in character. Geometry and periodicity are the origin of these effects, as these determine the polarizability, and coupling conditions, of the particles constituting the array [12, 15, 17].

#195021 - $15.00 USD Received 31 Jul 2013; revised 23 Sep 2013; accepted 24 Sep 2013; published 4 Nov 2013

4. Extinction of nanoparticle arrays with R6G molecules

We proceed with measurements of the same arrays but in the presence of R6G molecules. For this purpose we removed the PVA layer, and deposited a new PVA layer of the same thickness but doped with R6G molecules at 30 weight %. Figure 3 shows extinction measurements in this new system. The relevant bare states are now the upper SLR and the R6G exciton. The radiative coupling of these two states, which is determined by the spatial overlap of the associated electric fields, leads to the formation of two new states: the plasmon-exciton-polaritons (PEPs). We calculate the PEP eigenenergies in a similar manner as the SLR eigenenergies were calculated, using the following 2×2 Hamiltonian,

$$H_2 = \begin{pmatrix} E_X - i\gamma_X & \Omega_{XS} \\ \Omega_{XS} & E_{SLR} - i\gamma_{SLR} \end{pmatrix}. \tag{2}$$

Based on the absorption measurements of the bare R6G layer in Fig. 1(b), we set $E_X - i\gamma_X = (2.3 - i0.15)$ eV for the bare exciton energy. E_X is shown as black solid lines in Fig. 3. The complex SLR energy, $E_{SLR} - i\gamma_{SLR}$, is calculated from the diagonalization of H_1 in Eq. (1). E_{SLR} is shown as black dashed lines in Fig. 3. The mixed states (plasmon-exiton-polaritons) are obtained from the diagonalization of the Hamiltonian H_2 in Eq. (2), while the coupling constant Ω_{XS} was fitted to match the experiments. The resultant PEP energies are shown as black dash-dotted lines in Fig. 3. The calculated PEP dispersion agrees reasonably well with the measurements. The small disagreements are likely due to the simplicity of the model. In particular, we have used a constant Ω_{XS}, although this parameter is expected to vary with the wave vector because the field overlap between the modes changes. We note that González-Tudela and co-workers have recently demonstrated how to rigorously calculate the coupling between SPPs in a flat metallic layer and an ensemble of quantum emitters under the influence of decay and dephasing [34].

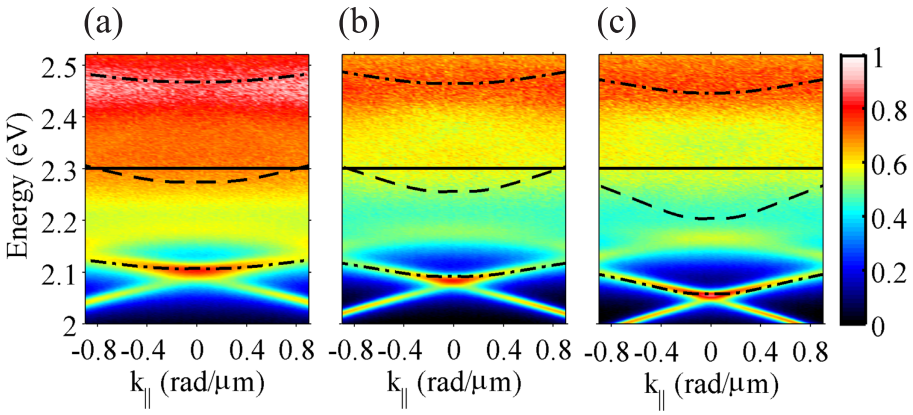

Fig. 3. Extinction of the same arrays in Figure 2, but here covered by a 300 nm layer of PVA doped with R6G at 30 weight %. The solid black line indicates the bare exciton energy, while the dashed black line indicates the upper SLR as calculated in Figure 2; these are the bare states. The dash-dotted black lines are the energies of the plasmon-exciton-polaritons, i.e., the eigenenergies of the Hamiltonian in Eq. (2); these are the coupled states. The lattice constants are (a) $a_x = 350$ nm, (b) $a_x = 360$ nm, and (c) $a_x = 370$ nm.

Fitting the PEP dispersion to the experiments yields the following values for the coupling constant: $\Omega_{XS} = 181 \pm 5$ eV for the $a_x = 350$ nm array, $\Omega_{XS} = 186 \pm 5$ eV for the $a_x = 360$ nm array, and $\Omega_{XS} = 191 \pm 5$ eV for the $a_x = 370$ nm array. While the changes in Ω_{XS} here reported

#195021 - $15.00 USD Received 31 Jul 2013; revised 23 Sep 2013; accepted 24 Sep 2013; published 4 Nov 2013

are small, we believe that the observed trend is physically plausible based on the following reasons. As discussed in the previous section, the SLR becomes less confined for increased lattice constants. This means that the electromagnetic field decays further out of the plane, thereby increasing the SLR coupling strength to excitons near the upper end of the R6G/PVA layer. Considering that Ω_{XS} represents an effective coupling strength between the molecular ensemble and the SLRs, this effective coupling can be expected to increase as the number of excitons participating in the coherent energy exchange increases.

The extinction measurements in Fig. 3 display interesting differences between the upper and lower PEP bands. The upper PEP has a peak energy, linewidth, and extinction that are nearly constant for all $k_{\|}$. In contrast, the lower PEP displays a variable dispersion, extinction, and linewidth. We attribute these differences to the properties of the underlying bare states: the upper SLR and the R6G exciton. Furthermore, as explained in the previous section, the SLR is itself a hybrid mode formed by the strong coupling between a LSPR and Rayleigh anomalies. At high energies the LSPR fraction in the upper SLR is higher. As the LSPR has a peak energy, linewidth, and extinction that are nearly constant for all $k_{\|}$, the SLR acquires similar properties when its energy is close to the LSPR energy. Thus, a similar effect occurs when the PEP energy approaches the energy of the LSPR underlying the SLR.

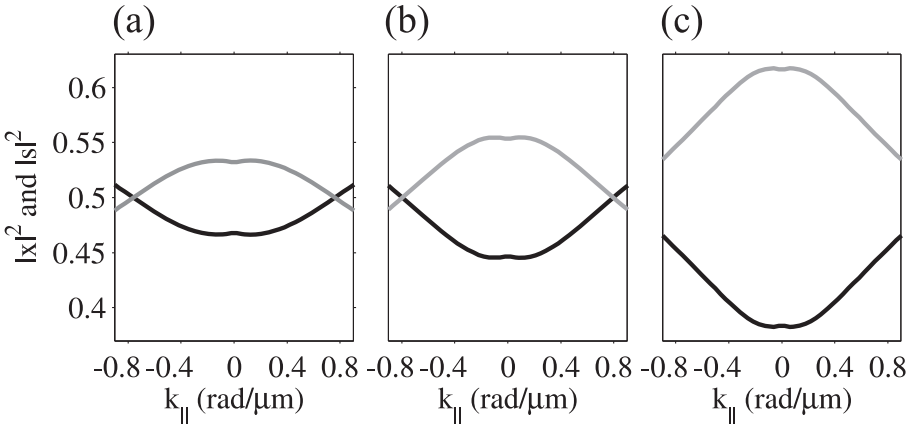

Fig. 4. Eigenstate fractions for the lower plasmon-exciton-polariton bands in Fig. 3 as a function of the incident wave vector. The black line represents the exciton fraction $|x|^2$, whereas the grey line represents the SLR fraction $|s|^2$. The lattice constants are (a) $a_x = 350$ nm, (b) $a_x = 360$ nm, and (c) $a_x = 370$ nm.

In what follows, we will concentrate on the lower PEP band. Let us analyze the composition of PEPs, which include SLR and exciton constituents depending on $k_{\|}$. We express the PEP eigenstates as $\left|\wp(k_{\|})\right\rangle = x(k_{\|})\,|X\rangle + s(k_{\|})\,|S\rangle$, with $|X\rangle$ and $|S\rangle$ the exciton and SLR states, respectively. The coefficients in the expansion of light-matter quasiparticles are often called the Hopfield coefficients [39], in honor to J.J. Hopfield, who: i) showed that excitons are approximate bosons (a key element enabling Bose condensates in excitonic systems), and ii) introduced the term "polariton" to describe the exciton-photon admixture [40]. Here, the Hopfield coefficients are the components of the eigenvector associated with the PEP's eigenenergy. The magnitude squared of the Hopfield coefficients yields the eigenstate fractions, or composition, of the admixture. We plot these in Figs. 4(a)- 4(c) for the lower PEP band in Figs. 3(a)- 3(c), with the exciton fraction $|x(k_{\|})|^2$ as a black line and the SLR fraction $|s(k_{\|})|^2$ as a gray line.

The PEP eigenstate fractions are increasingly out-balanced with just small changes in the periodicity of the array. For $a_x = 350$ nm, the PEP ground state is composed by SLR and exci-

#195021 - $15.00 USD Received 31 Jul 2013; revised 23 Sep 2013; accepted 24 Sep 2013; published 4 Nov 2013

ton constituents with roughly equal weights, whereas for $a_x = 370$ nm the SLR fraction (0.6) becomes more important. This influence of the periodicity on the PEP composition is related to the dispersive properties of the bare states underlying the PEPs. In particular, the lattice constant determines the detuning between the LSPR and Rayleigh anomalies forming the upper SLR. The LSPR-Rayleigh-anomaly detuning changes the dispersion of the upper SLR to which the excitons couple, and thus the dispersion of the PEPs is modified. This effect, combined with the fact that in the strong coupling regime there is a transmutation of the eigenmodes as the detuning of the bare states transits through zero (close to our experimental conditions), leads to a non-trivial dependence of the PEP eigenstate fractions on the lattice constant. Next, we analyze the influence of this change in composition on the plasmon-exciton-polariton properties.

In Fig. 5 we analyze the dispersion and linewidth of the lower PEP bands in the three arrays. For this purpose, we approximate the PEP lineshape at each wave-vector as a Lorentzian resonance, which we fit by a least-squares method to the measurements. Figure 5(a) shows an example of such fitting at $k_{\|} = 0$ to the lower PEP resonance of the three arrays. The data points are the measurements, and the black solid lines are the fits. The fits cover a limited energy range only (same range for all $k_{\|}$, different for each array) to exclude the influence of other resonances at $k_{\|} \neq 0$. We extract the central energy and full width at half maximum (FWHM $= 2\gamma$ with γ the damping) of the fitted Lorentzians as a function of $k_{\|}$, and we plot these in Fig. 5(b) and Fig. 5(c), respectively. In Figs. 5(a)-(c), the blue squares correspond to the $a_x = 350$ nm array, the gray circles to the $a_x = 360$ nm array, and the red triangles to the $a_x = 370$ nm array. The error bars in the central energy and FWHM represent a 2σ (95%) confidence interval in the fits.

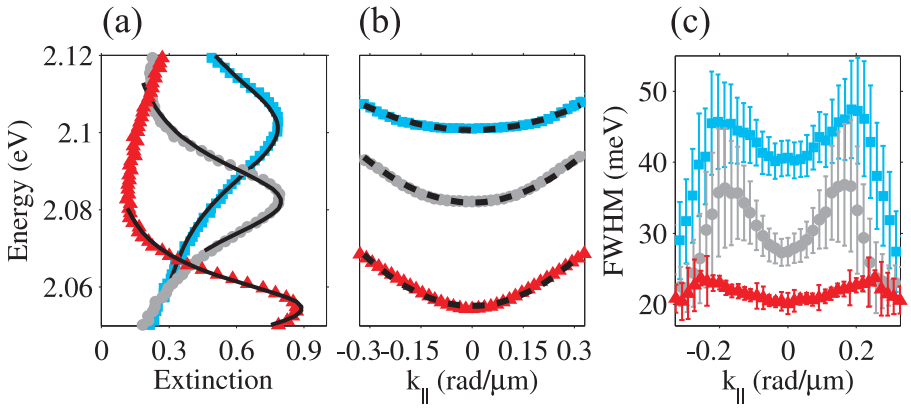

Fig. 5. (a) Extinction spectra at $k_{\|} = 0$, (b) dispersion relations, and (c) full width at half maximum (FWHM), of the lower plasmon-exciton-polariton in Figs. 3(a)-(c). The blue squares, grey circles, and red triangles in all figures correspond to the arrays in Figure 3(a), 3(b), and 3(c), respectively. Notice that the scales are different from Figure 2 and Figure 3. The error bars in (b) and (c) [smaller than the data points in (b)] represent a 2σ confidence interval in fitting the measured resonance with a Lorentzian lineshape at each $k_{\|}$. An example of such fitting procedure is shown in (a), where the fitted Lorentzians are shown as solid black lines. The dashed black lines in (b) are quadratic fits used to retrieve the plasmon-exciton-polariton effective mass.

In order to estimate the PEP effective mass, we approximate PEPs as free-quasiparticles in the low momentum regime. The black lines in Fig. 5(b) are fits of a quadratic function to the PEP dispersion near $k_{\|} = 0$. The good agreement between these quadratic fits and the PEP dispersion for the 3 arrays confirms that PEPs effectively behave as free-quasiparticles, with an effective mass $m^* = \hbar^2(\partial^2 E/\partial k_{\|}^2)^{-1}$. This yields $m^* = 5.4 \pm 0.3 \times 10^{-37}$ kg for $a_x = 350$ nm,

#195021 - $15.00 USD Received 31 Jul 2013; revised 23 Sep 2013; accepted 24 Sep 2013; published 4 Nov 2013

$m^* = 3.1 \pm 0.1 \times 10^{-37}$ kg for $a_x = 360$ nm, and $m^* = 2.6 \pm 0.1 \times 10^{-37}$ kg for $a_x = 370$ nm. The error in the mass represents a 2σ (95%) confidence interval in the quadratic fits to the dispersion relation in the plotted range. The changes in effective mass here observed are a manifestation of the changing PEP composition. As the PEP ground state energy is increasingly detuned from the bare exciton energy (the most heavy amongst the SLR and exciton), the effective PEP mass is reduced. The lightest of the three PEPs here analyzed is roughly 7 orders of magnitude lighter than the electron rest mass.

To assess the total loss rates of the PEPs, we plot their FWHM in Fig. 5(c). The FWHM is influenced by the periodicity of the array and by $k_{\|}$. From the increase of the FWHM with the lattice constant at any $k_{\|}$, it follows that the loss rates are primarily dictated by the periodicity. The origin of this dependence can be traced to the dependence of the SLR FWHM on the periodicity, as observed in Fig. 2. For shorter lattice constants the SLR FWHM is broadened by the increasingly dominant LSPR fraction (the most lossy amongst the underlying SLR constituents). Thus, the PEP FWHM is broadened accordingly. The PEP FWHM has a secondary dependence on $k_{\|}$, which is also based on the properties of the underlying SLR. For small $k_{\|}$, the mutual coupling between SLRs leads to pronounced changes in linewidth and dispersion [15]. Standing waves are formed in the upper SLR band, while subradiant damping sets in the lower SLR band. These $k_{\|}$-dependent changes in radiative damping are the origin of the variations in FWHM observed in Fig. 5(c). Certainly, Ohmic losses will set a lower limit on the FWHM, and this can drive the material of choice. Here we have used silver, which is well known for its low optical losses in the visible spectrum. However, we envisage that by fine tuning the geometry of the nanorods and the periodicity of the array, radiative losses can be minimized even further to yield PEPs with longer lifetimes.

The results in Fig. 4 and Fig. 5 demonstrate the opportunities and challenges that plasmon-exciton-polaritons may face in their way towards the quantum degeneracy threshold. For increasingly negative SLR-exciton detuning (larger lattice constant), the effective PEP mass is reduced and this is beneficial for increasing the critical temperature required for condensation. However, one should note that such an admixture has a reduced plasmonic and excitonic content at $k_{\|} = 0$. Another important parameter is the FWHM of the resonance, which also decreases for increasingly negative SLR-exciton detuning as shown in Fig. 5(c). The lifetime of the excitations (inversely proportional to the FWHM) is a key element to consider in the pursuit of a quantum condensate, as it will influence the dynamics (e.g. equilibrium vs non-equilibrium) of the system. In summary, we reckon the simultaneous decrease in linewidth and plasmonic content as a manifestation of the well-known trade-off between localization and losses in plasmonic systems.

5. Conclusion

In conclusion, we have investigated the strong coupling of surface lattice resonances in periodic arrays of metallic particles to excitons in Rhodamine 6G molecules. The properties of plasmon-exciton-polaritons (PEPs), the quasiparticles emerging from this coupling, were analyzed. We showed how the PEP effective mass, composition, and lifetime, can be tuned by varying the lattice constant of the array. We envisage these results to aid in the design of plasmonic systems that could open a yet un-explored but potentially rich avenue for plasmonics research: quantum condensation.

Acknowledgments

We thank Marc Verschuuren for the fabrication of the nanorod arrays, and Johannes Feist and Fracisco J. Garcia Vidal for stimulating discussions. This work was supported by the Netherlands Foundation for Fundamental Research on Matter (FOM) and the Netherlands Organiza-

tion for Scientific Research (NWO), and is part of an industrial partnership program between Philips and FOM.

#195021 - $15.00 USD Received 31 Jul 2013; revised 23 Sep 2013; accepted 24 Sep 2013; published 4 Nov 2013